Drug Delivery

DOI: 10.1002/anie.201411524

Antitumor Drug Delivery Modulated by A Polymeric Micelle with an Upper Critical Solution Temperature**

*Weishuo Li, Liwen Huang, Xiaoying Ying, You Jian, Yuan Hong, Fuqiang Hu, and Yongzhong Du**

Abstract: *Thermally sensitive polymeric nanocarriers were developed to optimize the release profile of encapsulated compounds to improve treatment efficiency. However, when referring to thermally sensitive polymeric nanocarriers, this usually means systems fabricated from lower critical solution temperature (LCST) polymers, which have been intensively studied. To extend the field of thermally sensitive polymeric nanocarriers, we for the first time fabricated a polymeric drug delivery system having an upper critical solution temperature (UCST) of 43 °C based on an amphiphilic polymer poly(AAm-co-AN)-g-PEG. The resulting polymeric micelles could effectively encapsulate doxorubicin and exhibited thermally sensitive drug release both in vitro and in vivo. A drastically improved anticancer efficiency (IC_{50} decreased from 4.6 to 1.6 $\mu g\,mL^{-1}$, tumor inhibition rate increased from 55.6 % to 92.8 %) was observed. These results suggest that UCST-based drug delivery can be an alternative to thermally sensitive LCST-based drug delivery systems for an enhanced antitumor efficiency.*

Targeted drug delivery systems (TDDSs) have gained more and more attention in recent years. They can significantly enhance the drug distribution in the tumor and avoid nonspecific drug distribution through the whole body, thereby improving the therapeutic index.[1–4] However, except for the selective drug delivery to the target sites, the TDDSs have an another important component: drug release control at the target sites, whose importance derives from the fact that a drug cannot exploit its pharmacological activities unless it is released from the carrier. Therefore, not only a selective drug delivery but also a controlled drug release that follows an appropriate rate and timing[5–8] are required to construct an ideal drug carrier.

One way to integrate the selective drug delivery and controlled drug release is the stimuli-responsive drug delivery system, which may include light-,[9] ultrasound-,[10] temperature-,[11] pH-,[12] and glutathione-[12]sensitive systems. Among all these stimuli-responsive drug delivery systems, the temperature-sensitive drug delivery system has gained more popularity, because the temperature change is easily and safely acquired.[13,14]

For temperature-responsive drug delivery systems, two types have been intensively studied: polymeric drug delivery systems fabricated from lower critical solution temperature (LCST) polymers and thermally sensitive liposomes.[14] Thermosensitive liposomes utilizing lipids that exhibit a phase transition temperature near 41 °C only facilitate drug release under temperature stimuli[14] but do not allow complete drug release. Furthermore, the thermoresponsive liposomes are not suitable for the encapsulation of water-insoluble drugs; The most studied LCST polymer is poly(*N*-isopropylacrylamide) (PNIPAm), which undergoes a sharp coil–globule transition in water at 32 °C, changing from a hydrophilic state below this temperature to a hydrophobic state above it.[15–17]

In contrast, the polymeric drug carriers exhibiting an upper critical solution temperature (UCST) have not been reported to our knowledge, which is due to the fact that the UCST of known examples is either sensitive to both electrolyte and polymer concentration[18] or demands a water/organic cosolvent[19,20] which makes them unsuitable for application in drug carriers. To extend thermoresponsive polymeric drug delivery systems, we fabricated a drug delivery system with a UCST of 43 °C based on an amphiphilic polymer poly(AAm-*co*-AN)-*g*-PEG, whose UCST relies on hydrogen bonding and its UCST behavior was independent of solvent, ionic strength, and polymer concentration.

Here, poly(AAm-*co*-AN)-g-PEG having a UCST of 43 °C was synthesized through a two-step process, and the synthetic route is shown in Figure 1 A. Poly(AAm-*co*-AN) was first synthesized by the solution copolymerization of acrylonitrile (AN) and acrylamide (AAm). The molar ratio of AAm/AN and the weight-average molecular weight of the obtained poly(AAm-*co*-AN) were 4.26:1 and 32.5 kDa, respectively (Figure S1A), and were obtained by adjusting the feed ratio of AM to AN and the amount of the initiator. Poly(AAm-*co*-AN)-g-PEG was subsequently synthesized through the reaction between the amide group of poly(AAm-*co*-AN) and the succinimide group of methoxy poly(ethylene glycol)succinimidyl carbonate-5 K (mPEG-SC-5K). The reaction mechanism is illustrated in Figure S1B and the structure of the final

[*] Dr. W. S. Li, Dr. L. W. Huang, X. Ying, Prof. Dr. Y. Jian, Prof. Dr. Y. Hong, Prof. Dr. F. Q. Hu, Prof. Dr. Y. Z. Du
College of Pharmaceutical Sciences, Hangzhou(China)
866 Yuhangtang Road, Hangzhou 310058 (China)
E-mail: duyongzhong@zju.edu.cn

[**] This study was supported by the National Natural Science Foundation of China (81373345) and the Nature Science Foundation of Zhejiang province (LZ13H300001).

Supporting information for this article including details of the synthesis and characterization of poly(AAm-co-AN)-g-PEG and drug-loaded poly(AAm-co-AN)-g-PEG as well as on the in vivo antitumor therapy is available on the WWW under http://dx.doi.org/10.1002/anie.201411524. All animal experiments were performed in accordance with the National Institutes of Health Guide for the Care and Use of Laboratory Animals with the approval of the Scientific Investigation Board of Zhejiang University, Hangzhou, China.

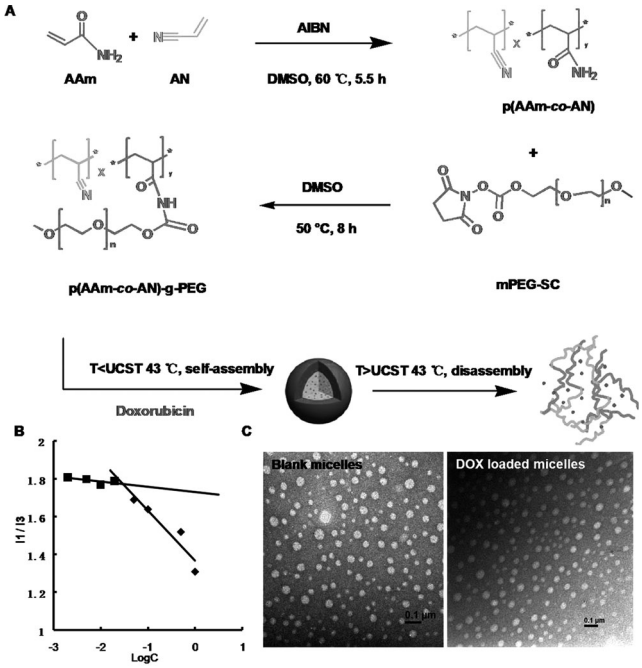

Figure 1. Fabrication and characterization of poly(AAm-*co*-AN)-*g*-PEG micelles. A) Synthesis of poly(AAm-*co*-AN)-*g*-PEG. B) Variations in the fluorescence intensity ratios of the first peak to the third peak for pyrene emission (I_1/I_3) against the logarithm of poly(AAm-*co*-AN)-*g*-PEG concentration. C) Transmission electron micrographs of blank and DOX-loaded micelles. Scale bars = 0.1 μm.

copolymer was confirmed using ^{1}H NMR (Figure S1B) and FTIR spectroscopy (Figure S1C); the weight-average molecular weight was determined to be 56.6 kDa, a significant increase compared to that of poly(AAm-*co*-AN) which indicates the successful grafting of mPEG-SC-5 K (Figure S1A). The graft ratio of PEG was estimated to be 1:4.82 based on the molecular weights, indicating that 4.82 PEG chains were present per poly(AAm-*co*-AN) chain.

The synthesized poly(AAm-*co*-AN)-g-PEG was found to self-assemble to micelles in aqueous solution at ambient temperature. The critical micelle concentration (CMC) was found to be 30.3 μg mL^{-1} (Figure 1 B). The doxorubicin base (DOX) was subsequently encapsulated into poly(AAm-co-AN)-g-PEG micelles by dialysis (drug content: 5.8 wt %). Transmission electron microscopy (TEM) images of blank and DOX-loaded micelles at 25 °C indicated that both micelles exhibited spherical shape with diameters of approximately 50 nm by number (Figure 1 C).

Dynamic light scattering was also performed to determine the hydrodynamic diameter of the micelles. Interestingly, as shown in Figure 2 A, the size of the micelles decreased as the temperature increased from 4 to 43 °C; when the temperature exceeded 43 °C, the size of the micelles was too small to detect. This phenomenon was also observed when a series of copolymer concentrations was used (50–1000 μg mL^{-1}; Figure 2 B). In response to the shift in temperature from 4 to 43 °C, the interlayer of the micelle underwent a transition from highly hydrophobic to hydrophilic, leading to a transition from poorly defined aggregates to more defined micellar structures. When the temperature reached 43 °C, the micelles disassembled. These results indicated that poly(AAm-*co*-AN)-*g*-PEG micelles exhibited a UCST near 43 °C in water and that the UCST was independent of copolymer concentration. Notably, after loading DOX, the micelles exhibited identical behavior (Figure 2 A). To further confirm this UCST behavior, turbidity measurements were conducted at 617 nm using UV/Vis spectroscopy. As shown in Figure 2 C, the transmittance of blank and DOX-loaded micelles increased as the temperature was increased from 4 °C to 43 °C; when the temperature exceeded 43 °C, the transmittance remained constant. This typical UCST behavior has been reported previously.[21] The temperature of 43 °C, at which the transmittance began to be constant, was defined as the UCST.

The drug release behavior was subsequently investigated using several methods to confirm the temperature-responsive feature of the micelles. Firstly, free DOX solution, and DOX-loaded micelles (DOX concentration: 30 μg mL^{-1}) were added into respective wells in an agarose gels, which were incubated at 37 °C and 43 °C for 30 min, followed by observation using an in vivo imaging system. As shown in Figure 2 D, the fluorescence intensity of the DOX-loaded micelles at 43 °C was much higher than that at 37 °C and was similar to that of free DOX (control). The fluorescence emission spectra of the samples were also determined (Figure 2 E). A fluorescence intensity that was similar to free DOX was observed for the DOX-loaded micelles at 43 °C, whereas the blank micelles exhibited negligible fluorescence at 565 nm. Reverse dialysis methods, which are analogous to the conditions presented following i.v. administration of the formulation, were also conducted to further confirm this temperature-sensitive behavior. As shown in Figure 2 F, a temperature of 43 °C induced rapid and complete DOX release from the DOX-loaded micelles, which exhibited a drug release profile that was similar to that of free DOX (37 and 43 °C). In contrast, the release of DOX from the DOX-loaded micelles at 37 °C was slow and incomplete during the evaluated period similar to that of conventional micelles. Both the higher DOX fluorescence of the DOX-loaded micelles and the improved drug release profile at 43 °C may be explained by the disassembly of the micelles at 43 °C that resulted in a higher free DOX concentration in the release medium.

The internalization of the DOX-loaded micelles was investigated using BEL-7402 cells as a model human hepatic carcinoma cell line. As shown in Figure 3 A, following cell exposure to DOX-loaded micelles, the micelles transported DOX into tumor cells, including into the nucleus. The cellular uptake of free DOX was displayed in Figure S2. The average optical density (AOI) of the pictures of DOX-loaded micelles and free DOX at 24 h was 12.235 and 13.571, respectively.

The cytotoxicity of the blank and DOX-loaded micelles was subsequently estimated using the 3-(4,5-dimethylthiazol-2-yl)-2,5-diphenyltetrazolium bromide (MTT) assay. As shown in Figure 3 B, the blank micelles (left) appeared to exhibit low cytotoxicity, as the cell viability exceeded 80 % at micelle concentrations of up to 1 mg mL^{-1}; hyperthermia did not affect the cell viability. The cell viability following treatment with DOX-loaded micelles (right) was significantly

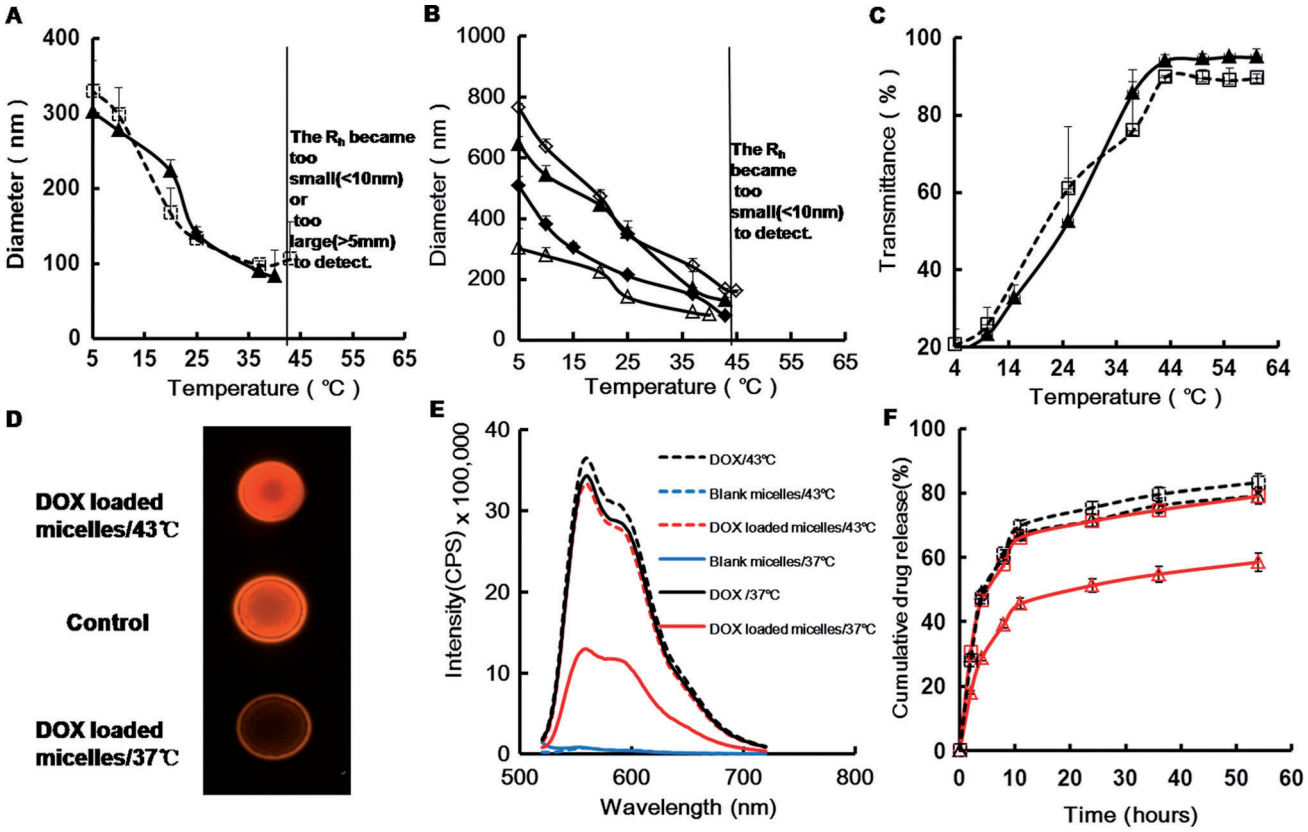

Figure 2. Thermosensitive behavior of the micelles. A) Size distribution of the blank (▲) and DOX-loaded micelles (□) in response to a shift in temperature from 4 °C to 43 °C. B) Variations in the micelle size as a function of temperature at various copolymer concentrations (▲: 0.05 mg mL^{-1}; ◆: 0.1 mg mL^{-1}; ▲: 0.5 mg mL^{-1}; ◇: 1 mg mL^{-1}). C) Transmittances of the blank (▲) and DOX-loaded micelles (□) as a function of temperature. D) Fluorescence images of free DOX (control) and the DOX-loaded micelles following incubation at 37 and 43 °C. E) Fluorescence emission spectra of the blank micelles, free DOX, and DOX-loaded micelles following incubation at 37 or 43 °C. F) In vitro drug release profiles of free DOX (black △: 37 °C, black □: 43 °C) and the DOX-loaded micelles at 37 °C (red △) and 43 °C (red □). The results represent the mean values ± S.D. In the cases in which the error is not visible, the error was small.

reduced upon hyperthermia. The 50 % cellular inhibition (IC_{50}) value of the hyperthermic group of DOX-loaded micelles was approximately 1.56 μg mL^{-1}, compared with that in the absence of hyperthermia (4.91 μg mL^{-1}). However, the cytotoxicity of free DOX did not show any significant difference with or without hyperthermia (from 4.32 to 4.65 μg mL^{-1}). Figure 3 C shows the stained images of living cells following treatment of the cells with free DOX and DOX-loaded micelles followed by hyperthermia. As shown in Figure 3 C, the number of viable cells in the group that was exposed to hyperthermia alone was similar to that in the control group, which suggested that hyperthermia alone did not affect cell viability in vitro and was consistent with previous report.[22] However, the group exposed to DOX-loaded micelles and hyperthermia exhibited the fewest viable cells in comparison to all of the other groups, indicating an excellent antitumor effectiveness. The encapsulated DOX was assumed to be immediately and completely released in the cells following hyperthermia. Consequently, the substantial increase in the free DOX concentration at the target site resulted in high cytotoxicity.

To confirm this assumption, Nile red was encapsulated into the micelles instead of DOX to evaluate intracellular drug release. Fluorescence from Nile red cannot be observed unless it is released from the micelles and interacts with lipids in the cytosol.[23] As shown in Figure 3 D, cells that had been treated with Nile-red-loaded micelles and hyperthermia exhibited much stronger Nile red fluorescence than the cells that had been incubated with Nile-red-loaded micelles without hyperthermia treatment. Quantitative analysis using flow cytometry (Figure 3 E) showed similar results, which confirmed that the intracellular drug release from the micelles could be highly accelerated by hyperthermia.

To investigate the passive targeting ability of the micelles, the fluorescent dye indocyanine green (ICG) complexed with tetrabutylammonium iodide was encapsulated in the micelles, and the in vivo distribution was examined using nude mice bearing BEL-7402 tumor. As shown in Figure S3A, the mouse showed a strong fluorescence signal throughout the whole body for up to 4 h post-injection. Thereafter, the fluorescence intensity of ICG in tumor tissues increased from 6 to 24 h, indicating a long circulation and passive tumor targeting ability. After 24 h, the fluorescence intensity in tumor tissues was reduced gradually.

Ex vivo fluorescence evaluation of the harvest organs and tissues at 48 h post-injection also confirmed the increased

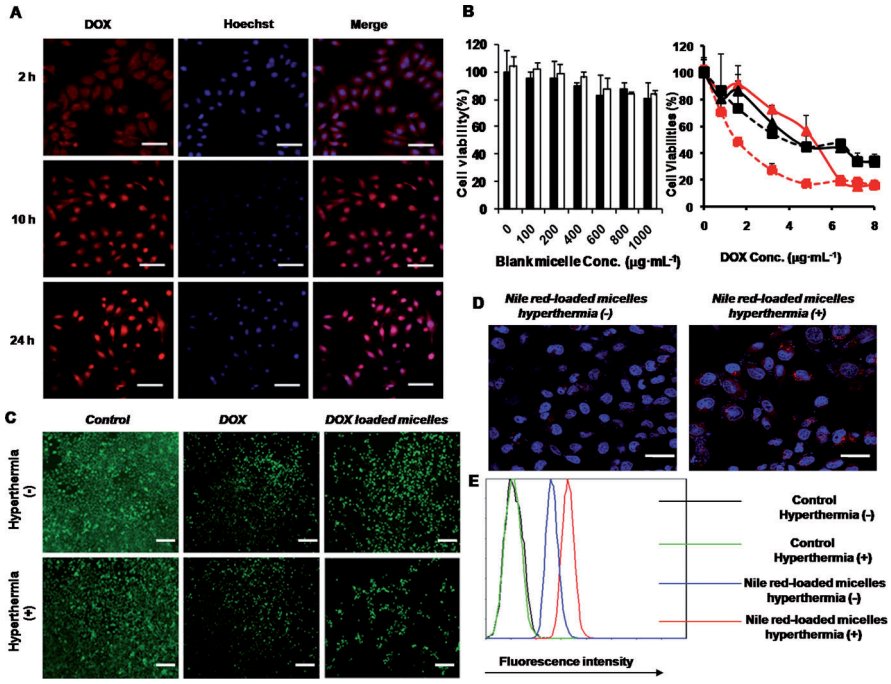

Figure 3. Biological studies of the DOX-loaded micelles on BEL-7402 cells. A) Confocal laser scanning microscopic images of BEL-7402 cells incubated with DOX-loaded micelles for different periods of time (scale bar = 14 μm; blue: Hoechst 33342; red: DOX). B) Variations in BEL-7402 cell viability as a function of the concentration of blank micelles in the presence (□) or absence (■) of hyperthermia, DOX-loaded micelles in the presence (red ■) or absence (red ▲) of hyperthermia and DOX in the presence (black ■) or absence (black ▲) of hyperthermia. The results represent the mean values ± S.D. C) Fluorescence images of live BEL-7402 cells without DOX, with DOX, or with DOX-loaded micelles in the presence (+) or absence (−) of hyperthermia (scale bar = 200 μm). D) Confocal laser scanning microscopic images of BEL-7402 cells incubated with Nile-red-loaded micelles in the absence (left) or presence (right) of hyperthermia (red: Nile red; blue: Hoechst 33342; scale bar = 30 μm). E) Fluorescence intensity within BEL-7402 cells following exposure to Nile-red-loaded micelles in the presence or absence of hyperthermia.

accumulative ICG-loaded micelles in the tumor (Figure S3B). This selective accumulation in the tumors resulted from surface PEGylation[24] and the "EPR" effect.[25] To validate the therapeutic efficacy of this temperature-responsive system, a microwave therapy apparatus was utilized to induce hyperthermia in vivo. An approximately 6 °C increase in the temperature of the tumor tissue was observed after the mouse was exposed to microwave radiation (2450 MHz, 8 W) for 30 min (Figure S4), which met the requirements for microwave hyperthermia and the temperature sensitivity of the micelle.

As indicated in Figure 4A, changes in the tumor volume occurred following the first administration. In all of the evaluated groups, no significant body weight changes were observed (Figure S5A). The tumor volume in the blank micelle group was similar to that in the saline group, indicating that the blank micelles did not have an antitumor effect. However, the use of microwave radiation alone demonstrated partial efficiency, as the final volume was smaller than that of the saline group and the tumor inhibition rate was approximate 42.8%. Adriamycin, a commercial DOX preparation, could suppress the tumor growth. However, no significant difference was observed between the Adriamycin-treated groups in the presence or absence of microwave therapy, indicating the absence of a synergistic therapeutic effect for chemotherapy and hyperthermia. The tumor inhibition rates in the Adriamycin-treated groups in the presence and absence of microwave therapy were 87.7% and 82.3%, respectively. Although the DOX-loaded micelles accumulated in the tumor tissue, the final tumor volume was larger than that in the Adriamycin-treated groups, and the tumor inhibition rate was only 55.6%. This result may be explained by sustained drug release from the micelles inside the tumor cells. Notably, tumors in 50.0% of the nude mice in the group treated with DOX-loaded micelles and hyperthermia were entirely eradicated 18 days after the first treatment (Figure 4B), and the final tumor inhibition rate reached 92.8%. The highly improved antitumor efficiency may be due to rapid, complete and burst drug release after microwave exposure, and consequently lead to a deep drug penetration into the tumor center.

To verify this assumption, Nile-red-loaded micelles were administered. As shown in Figure 4C, Nile red fluorescence was observed throughout the tumor tissue in the microwave hyperthermic group. In contrast, low levels of Nile red fluorescence were observed on the edges of the tumor tissues when only Nile red-loaded micelles were administered. This may be explained by the high drug concentration gradient and decreased particle size assisting a deep tumor penetration.

As shown in Figure 4D, the most severe tumor cell necrosis was observed in the group treated with DOX-loaded micelles in combination with microwave therapy, whereas the Adriamycin-treated groups exhibited active tumor cell growth in certain regions of the tumor (red arrows, Figure S5B). This finding indicated that tumor recurrence had occurred in the late stage of the Adriamycin-treated groups. However, no active tumor cell growth was observed in the group treated with DOX-loaded micelles in combination with microwave therapy. This result may be due to the higher free drug concentration and deep penetration of the drug providing a possibility to kill the hypoxic tumor cells in the center of the tumors where the most aggressive tumor cells, stem cells, are located that can regenerate the tumor after therapy.[26] Based on the images of the hearts and livers (Figure 4D), the organs appeared to be normal, without obvious histopathological abnormalities, degeneration, or lesions in the micelle-

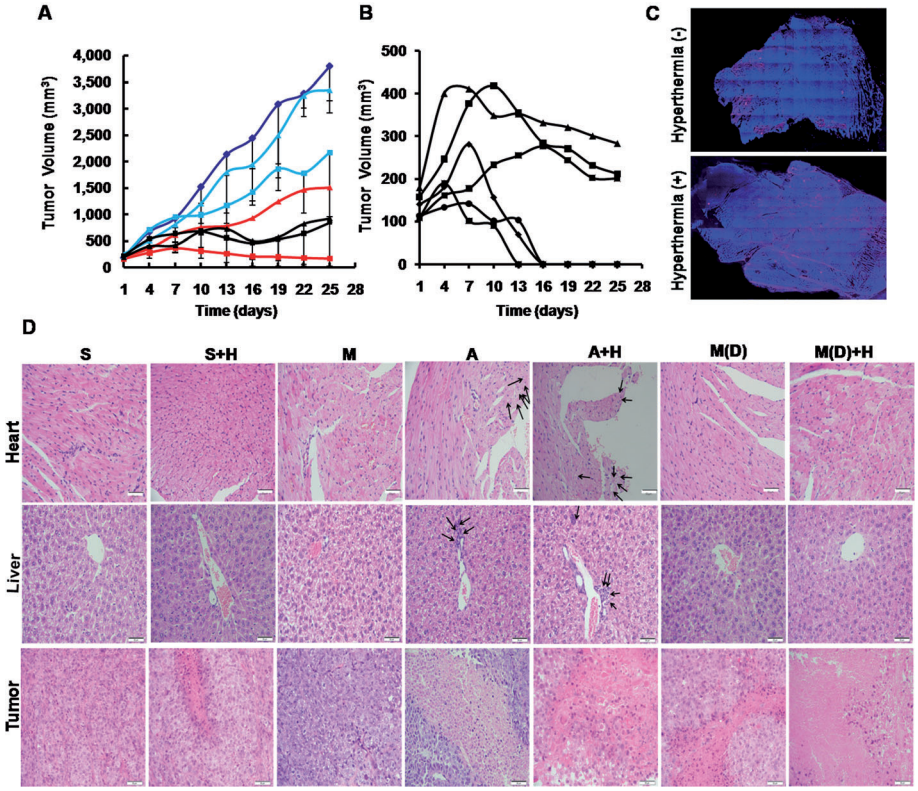

Figure 4. In vivo antitumor efficiency of DOX-loaded micelles. A) Tumor volume of the different treatment groups as a function of time. The results represent the mean values ± S.D. Squares indicate the hyperthermic groups (red ■: DOX-loaded micelles, M(D) + H; black ■: Adriamycin, A + H; pale blue ■: saline, S + H), and triangles represent the groups in the absence of hyperthermia (red ▲: DOX-loaded micelles, M(D); black ▲: Adriamycin, A; pale blue ▲: saline, S; blue ▲: blank micelles, M). B) Individual tumor growth curves from M(D) + H treatment groups. C) Fluorescence images of histological sections of the tumors 24 h post-i.v. injection of Nile-red-loaded micelles in the presence or absence of hyperthermia (blue: DAPI; red: Nile red; scale bar = 2 mm). D) Microscopic images of H&E-stained cross-sections of the tumors, livers, and hearts (25 days after the first treatment). Scale bar = 50 μm.

treated groups, indicating that no cellular or tissue damages had occurred. In contrast, serious cardiotoxicities (black arrows, Figure 4D) were induced by Adriamycin treatment, as indicated by the observed hyperaemia and myocardial fiber breakage, which were accompanied by acute inflammatory cell infiltration. Acute inflammatory cell infiltration (black arrows, Figure 4D) was also observed in the livers of the mice in the Adriamycin-treated groups.

In conclusion, we not only for the first time synthesized an amphiphilic UCST polymer displaying thermally sensitive behavior in water, but also explored its potential as a drug delivery agent. This novel drug delivery system could effectively encapsulate a hydrophobic antitumor drug and achieve a long systemic circulation after accomplishing the delivery task, the UCST carriers could continue to modulate the drug release by controlling the temperature in the tumor. Combined with microwave hyperthermia, a good antitumor outcome was achieved. This temperature-triggered poly(AAm-*co*-AN)-g-PEG micelles expand the temperature-triggered drug delivery systems and can potentially be applied for the treatment of cancer. Additionally, the temperature-triggered drug delivery system we fabricated is desirable for the treatment of circadian disease, pain attack, and infections which demand a high free-drug concentration in a short time.

Received: November 29, 2014
Published online: February 4, 2015

Keywords: controlled drug release · polymeric micelles · drug delivery · tumor therapy · upper critical solution temperature

[1] T. M. Allen, P. R. Cullis, *Science* **2004**, *303*, 1818 – 1822.
[2] F. Danhier, O. Feron, V. Préat, *J. Controlled Release* **2010**, *148*, 135 – 146.
[3] R. Duncan, *Nat. Rev. Drug Discovery* **2003**, *2*, 347 – 360.
[4] D. Peer, J. M. Karp, S. Hong, O. C. Farokhzad, R. Margalit, R. Langer, *Nat. Nanotechnol.* **2007**, *2*, 751 – 760.
[5] N. Huebsch, C. J. Kearney, X. H. Zhao, J. Kim, C. A. Cezar, Z. G. Suo, D. J. Mooney, *Proc. Natl. Acad. Sci. USA* **2014**, *111*, 9762 – 9767.
[6] J. Kopeček, *Adv. Drug Delivery Rev.* **2013**, *65*, 49 – 59.
[7] A. A. Cohen, N. G. Zatorsky, E. Eden, M. F. Morgenstern, I. Issaeva, A. Sigal, R. Milo, C. C. Saidon, Y. Liron, Z. Kam, *Science* **2008**, *322*, 1511 – 1516.
[8] K. A. Janes, J. G. Albeck, S. Gaudet, P. K. Sorger, D. A. Lauffenburger, M. B. Yaffe, *Science* **2005**, *310*, 1646 – 1653.
[9] L. F. Chen, W. Q. Wang, B. Su, Y. Q. Wen, C. B. Li, Y. B. Zhou, M. Z. Li, X. D. Shi, H. W. Du, Y. L. Song, L. Jiang, *ACS Nano* **2014**, *8*, 744 – 751.
[10] S. K. Cool, *J. Controlled Release* **2013**, *172*, 73 – 80.
[11] W. Li, W. Q. Wang, B. Su, Y. Q. Wen, C. B. Li, Y. B. Zhou, M. Z. Li, X. D. Shi, H. W. Du, Y. L. Song, L. Jiang, *Biomaterials* **2011**, *32*, 3832 – 3844.
[12] Y. J. Pan, Y. Y. Chen, D. R. Wang, C. Wei, J. Guo, D. R. Lu, C. C. Chu, C. C. Wang, *Biomaterials* **2012**, *33*, 6570 – 6579.
[13] S. A. Stanley, J. E. Gagner, S. Damanpour, M. Yoshida, J. S. Dordick, M. F. Jeffrey, *Science* **2012**, *336*, 604 – 608.
[14] J. H. Park, G. Maltzahn, L. L. Ong, A. Centrone, T. A. Hatton, E. Ruoslahti, S. N. Bhatia, M. J. Sailor, *Adv. Mater.* **2010**, *22*, 880 – 885.
[15] M. Y. Kim, B. Jung, J. H. Park, *Biomaterials* **2012**, *33*, 668 – 678.
[16] Z. C. Zhu, N. Gao, H. J. Wang, S. A. Sukhishvili, *J. Controlled Release* **2013**, *171*, 73 – 80.
[17] C. D. H. Alarcón, S. Pennadam, C. Alexander, *Chem. Soc. Rev.* **2005**, *34*, 276 – 285.
[18] D. N. Schulz, D. G. Peiffer, P. K. Agarwal, J. Larabee, J. J. Kaladas, L. Soni, et al., *Polymer* **1986**, *27*, 1734 – 1742.
[19] W. M. Wan, F. Cheng, F. Jäkle, *Angew. Chem. Int. Ed.* **2014**, *53*, 8934 – 8938; *Angew. Chem.* **2014**, *126*, 9080 – 9084.
[20] A. Can, S. Hoeppener, P. Guillet, J. F. Gohy, R. Hoogenboom, U. S. Schubert, *Polym. Chem.* **2011**, *49*, 3681 – 3687.

[21] J. Seuring, S. Agarwal, *Macromolecules* **2012**, *45*, 3910 – 3918.
[22] Y. Li, S. Pan, W. Zhang, Z. Du, *Nanotechnology* **2009**, *20*, 065 – 104.
[23] P. Greenspan, E. P. Mayer, S. D. Fowler, *J. Cell Biol.* **1985**, *100*, 965 – 973.
[24] T. M. Allen, *Nat. Rev. Drug Discovery* **2002**, *2*, 750 – 763.
[25] D. Papahadjopoulos, A. Gabizon, E. Mayhew, K. Matthay, S. K. Huang, K. D. Lee, M. C. Woodle, D. D. Lasic, C. Redemann, *Proc. Natl. Acad. Sci. USA* **1991**, *88*, 11460 – 11464.
[26] J. E. Visvader, G. J. Lindeman, *Nat. Rev. Cancer* **2008**, *8*, 755 – 768.

